PHILOSOPHICAL TRANSACTIONS A

royalsocietypublishing.org/journal/rsta

Research

Cite this article: Hiltner L, Calderer MC, Arsuaga J, Vázquez M. 2021 Chromonic liquid crystals and packing configurations of bacteriophage viruses. *Phil. Trans. R. Soc. A* **379**: 20200111.
https://doi.org/10.1098/rsta.2020.0111

Accepted: 1 December 2020

One contribution of 10 to a theme issue 'Topics in mathematical design of complex materials'.

Subject Areas:
applied mathematics, biomathematics, mathematical modelling, materials science

Keywords:
chromonic liquid crystals, bacteriophage virus, toroidal clusters, polyconvex functions, absoltue minimizer, solid–liquid transition

Author for correspondence:
M. Carme Calderer
e-mail: calde01@umn.edu

Chromonic liquid crystals and packing configurations of bacteriophage viruses

Lindsey Hiltner[1], M. Carme Calderer[1], Javier Arsuaga[2,3] and Mariel Vázquez[4,5]

[1]School of Mathematics, University of Minnesota, Minneapolis, MN 55442, USA
[2]Department of Cellular and Molecular Biology, Briggs Hall, Davis, CA 09
[3]Department of Mathematics, MSB, 2115, and [4]Department of Mathematics, MSB, 2150, University of California Davis, One Shields Avenue, Davis, CA 95616, USA
[5]Department of Microbiology and Molecular Genetics, Briggs Hall, Davis, CA 09

MCC, 0000-0002-9117-7439

We study equilibrium configurations of hexagonal columnar liquid crystals in the context of characterizing packing structures of bacteriophage viruses in a protein capsid. These are viruses that infect bacteria and are currently the focus of intense research efforts, with the goal of finding new therapies for bacteria-resistant antibiotics. The energy that we propose consists of the Oseen–Frank free energy of nematic liquid crystals that penalizes bending of the columnar directions, in addition to the cross-sectional elastic energy accounting for distortions of the transverse hexagonal structure; we also consider the isotropic contribution of the core and the energy of the unknown interface between the outer ordered region of the capsid and the inner disordered core. The problem becomes of free boundary type, with constraints. We show that the concentric, azimuthal, spool-like configuration is the absolute minimizer. Moreover, we present examples of toroidal structures formed by DNA in free solution and compare them with the analogous ones occurring in experiments with other types of lyotropic liquid crystals, such as food dyes and additives.

This article is part of the theme issue 'Topics in mathematical design of complex materials'.

THE ROYAL SOCIETY PUBLISHING

1. Introduction

This article deals with modelling and analysis of lyotropic chromonic liquid crystals, whose phases are found in biological systems, such as condensed DNA *in vitro* and in the spooling arrangements of double-stranded (ds)DNA in bacteriophage viruses, known to attack bacteria. We study equilibrium configurations of (ds)DNA in capsid domains, formulated as free boundary problems of the proposed packing energy. The very large bending resistance of the (ds)DNA inside the capsid allows for a well ordered, spool-like arrangement near the capsid boundary, subsiding into a disordered, isotropic core towards the centre of the capsid, whose interface with the former organized part is unknown. In our analysis, we treat it as a free boundary. We apply methods of calculus of variations to show existence of a unique energy minimizer corresponding to the concentric, azimuthal, spool-like configuration. We also address toroidal structures made by DNA in free, *in vitro* solutions as well as those found in chromonic samples of dyes and food additive compounds, whose sizes are about 10^5 to 10^6 times larger than their DNA analogues.

In addition to nucleotide, proteins, DNA and RNA, materials such as dyes, food additives (e.g. the dye Sunset Yellow), and pharmaceutical products also form chromonic structures with sizes about 10^6 times larger than those of their biological counterparts [1,2]. The chromonic denomination of liquid crystals emerges directly from the discovery that clustered DNA, in free solution and *in viva*, forms liquid crystal phases [3–5].

Lyotropic chromonic liquid crystals (LCLCs) differ significantly from the typical liquid crystals found in displays, which have long, rod-like molecules and change phase at well-known temperature thresholds. On the other hand, LCLCs consist of water-soluble, plank-like molecules with rigid cores and ionic groups at the periphery that can reversibly assemble into columns by stacking face to face; the length of these columnar aggregates varies strongly with temperature, concentration, and ionic content [6]. As the concentration of these molecules increases, the columns tend to elongate and align parallel to each other, forming a columnar nematic phase. As the concentration further increases, the more organized hexagonal columnar phase appears with the long axes of the columns forming a two-dimensional hexagonal lattice (figure 1). With the addition of condensing agents, such as (PEG) Polyethylene glycol and spermidine, the columns rearrange into toroidal aggregates. Double-stranded DNA in free solution also forms toroidal aggregates in the presence of condensing agents, but with clusters of sizes five orders of magnitude smaller than the former.

Another important natural setting in which the hexagonal columnar structure is exhibited is in bacteriophage viruses, where the (ds)DNA is tightly packed within. These viruses consist of a protein shell, capsid, and a tail with protein receptors or a connector structure used in infecting bacteria (figure 2). The life cycle of bacteriophages begins when DNA is spooled into an early form of capsid using a molecular motor while still in a bacterial host cell. The fully formed bacteriophages then destroy the host and leave to seek a live bacterium in which to replicate. Once the receptors on the tail detect a viable host, a reaction occurs that causes the DNA to be injected into the host, using the built up pressure within to release it. The bacteriophages take over the DNA replication mechanism of the host and copy their own DNA, which occurs rapidly since the viruses have much smaller genomes than the mechanism is made to handle, and the process begins again.

Bacteriophages are unique in that, with few exceptions, only their genome enters the host cell; in almost all other viruses, the entire virus structure enters the cell cytoplasm [11]. This suggests that the DNA within the bacteriophage capsid must be optimally packed for ejection, with pressures strong enough to inject the genome into the host cell. Typical bacteriophages measure about 50 nm in diameter and sustain internal pressures of around 30 to 60 atmospheres. This build up of pressure is caused by the confinement imposed on the DNA by the capsid, the bending rigidity of the DNA filament, and the electrostatic self-repulsion between the highly negatively charged DNA segments. The arrangement of the DNA inside the capsid encompasses a compactly packed, ordered region starting at the capsid wall, with a disordered, isotropic core formed to relieve the high bending energy due to the large persistence length of the DNA,

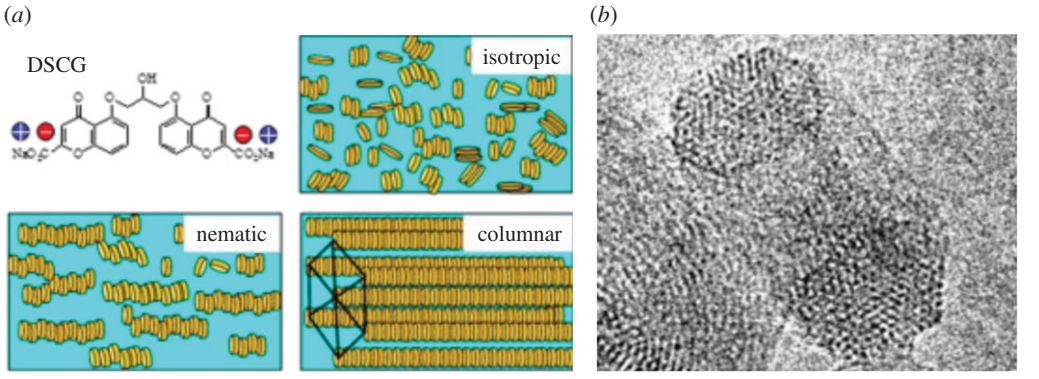

Figure 1. Chromonic molecule of disodium cromoglycate, Sunset Yellow and mesophases, it forms in water through aggregation [2] (*a*). Experimental image of a DNA toroidal condensate from [7] (*b*). (Online version in colour.)

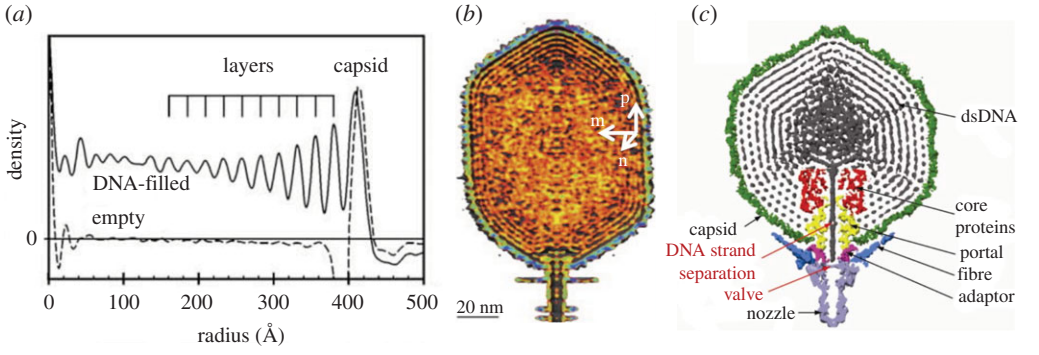

Figure 2. Density profile of the T5 virus [8] (*a*). Cryo-EM reconstruction of the T4 virus [9]. The DNA segments in the spooling configuration are perpendicular to the image, along the direction of the vector **n**, showing the orthonormal set (**n**, **m**, **p**) (*b*). The image on (*c*) shows the connector structure of the ϵ15 virus [10]. The connector is the structure that includes the core proteins, portal, fibre and adaptor. (Online version in colour.)

comparable to the capsid size. The proposed model, with energy contributions assigned to both the ordered and disordered regions, follows the point of view that the phase transition solid to fluid, as named by some authors, is an important functional feature of the bacteriophages [12], and especially relevant to the packing and release events.

It is predicted that technologies using phages—such as delivering genes that cause toxicity to target cells, inhibiting bacterial processes like replication, and detecting pathogens in hospital surfaces and food preparation—could aid or replace antibiotics in impeding highly resistant strains of disease causing bacteria [13]. With the number of potential applications of both naturally-occurring and synthesized bacteriophages growing every day, the ability to understand, accurately describe, and simulate certain phenomena associated with these objects is of increasing interest [14].

Mathematical models have been proposed to describe the packing of DNA in viruses [5,11,15–17] with energy functionals taken from the study of DNA molecules in free solution that do not account for possible liquid crystalline phases. Other research approaches that also incorporate liquid crystal phases but not necessarily within an energetics perspective have been developed [18,19], as well as works based on DNA helical arrangements [20]. In previous work, we investigated a model of liquid crystals with variable degree of orientation that enabled a characterization of the disordered core in terms of the nematic order parameter, and also allowing

for the identification of defects. The main feature of the study was the setting of a finite-element algorithm as a main tool for prediction and design [21].

The utility of a well-tuned continuum model includes the ability to accurately and reproducibly predict features of the system, such as pressure within a capsid, equilibrium shapes of aggregates, or the amount of disordered material coexisting with ordered material.

The energy density of a chromonic liquid crystal includes the Oseen–Frank energy of the nematic liquid crystal phase that penalizes bending of the columns, together with an elastic energy that accounts for distortions of the cross-sectional lattice perpendicular to the columnar directions at each point of the domain. Chromonic configurations are described by a set of linearly independent unit vectors, $\mathbf{n}$, $\mathbf{m}$ and $\mathbf{p}$. The nematic director $\mathbf{n}$ represents the average direction of column arrays at a point, and $\mathbf{m}$ and $\mathbf{p}$ denote the lattice vectors of the local cross-section. As in the modelling of rigid rod systems, defects correspond to points, lines, or surfaces with $\mathbf{n} = \mathbf{0}$, that is where the order is lost, with the material becoming locally isotropic. The main difficulty with the Oseen–Frank theory used in our work is in the modelling of two-dimensional configurations since it assigns infinite energy to point defects in the plane. In this paper, we also ignore the presence of defects and knots in the viral genome arrangements.

In addition to the Oseen–Frank energy that penalizes bending of the columnar axes, the elastic energy that we adopt to model distortions of the columnar cross-sections is motivated by the form proposed by de Gennes [22] but formulated to describe elastic materials made of filaments. Hence, we write it in terms of gradients of the lattice vectors $\mathbf{m}$ and $\mathbf{p}$, with the resulting expression involving the bulk and shear moduli of the chromonic material. The total energy to describe DNA viral packing also includes the penalty associated with the isotropic core and the surface energy of the interface between the ordered and the disordered part of the configuration.

The analysis addresses the minimization of the packing energies subject to multiple constraints, either in their exact or in their relaxed form. These leads to a free boundary problem for a polyconvex energy functional. The constraints involved are of geometric type, including those that reflect the rigidity of the material to splay and twist deformations, the hexagonal structure of the lattice, and the conservation of mass. The elastic energy is particularly relevant to the modelling of DNA encapsidation, due to the polymeric structure of the DNA molecule, with persistence length of the same order of magnitude as the capsid size. This results on high bending configurations of the well-ordered DNA region and forces a disordered core, towards the centre of the capsid, that we take as being in the isotropic liquid crystal phase. We assume that the capsid is an axisymmetric domain and neglect its polyhedral structure. Although some viruses present a chiral arrangement, this analysis focuses on standard spooling configurations around the capsid axis. In fact, it is found that among the set of admissible configurations, the planar, azimuthal, spool-like configuration is the unique minimizer. The shape of the core depends on the physical parameters of the model, and in particular, the bending rigidity of the DNA.

Determining the appropriate parameter ranges of the effective coefficients of the model involves three types of data. First of all, the size of the disordered core and density graphs revealing the ordered and disordered mass distribution in the capsid are available, for some viruses, as (CryoEM) cryogenic electron microscopy images. The length of the genome L, the effective DNA filament diameter d (it accounts for electrostatic repulsion), its persistence length L_p and the size of the capsid R_c are also available for many viruses. In particular, these values allow us to estimate the bending modulus K_3. We also appeal to the dimensional estimates of the compression and shear moduli of the hexagonal elastic energy, C and B, respectively, in terms of K_3 as proposed in [23]. We explore values for the isotropic modulus ν and the surface tension σ using Onsager's theory of rigid rods [24]. Finally, by finding the optimal size of the disordered core and matching its imaging value, we complete the selection of the effective coefficients of the model for a set of four viruses.

Among the most relevant shortcomings of the proposed model, we mention the fact that the distance, d, between neighbouring DNA segments within the ordered region of the capsid is not constant. In the case of toroidal domains, this has been pointed out in recent work by Barberi *et al.* [25]. Such a distance is also very sensitive to changes in ionic conditions [26].

Incorporating the Lénard-Jones potential used in the latter reference to the present model would allow us to treat d as an additional scalar variable, coupled with the bending energy through the constant K_3, and therefore having a direct impact on the core size. Furthermore, the ability to increase d plays a main role in genome delivery, as a mechanism fostering the solid-to-liquid transition, relevant to a successful infection [12]. A second shortcoming is neglecting possible defects that naturally occur in hexagonal chromonic lattices as well as ignoring the role of chirality [27,28]. These may affect the genome's delivery process leading to potential *jamming*.

This article is organized in the following way. In §2, we provide some background on LCLCs phases and present the model to be studied. We also provide modelling examples of *in vitro* DNA toroidal clustering. We first analyse limiting cases in which either the bending or surface tension is dominant, produce examples of equilibrium shapes for each setting, and compare them to experimental measurements. We find that the bending energy dominates in the case of DNA clusters whereas surface tension prevails in the case of chromonic dyes [6,29]. A modified model for DNA packed in a bacteriophage capsid is presented in §3, as well as an explanation of prior work in this area, describing the location of the DNA filament, and accounting for the self-repulsion of the spooled DNA. In §4, we consider a class of spheroidal disordered cores and prescribe the tangent field $\mathbf{n}$ to the DNA segments. This provides an energy that is minimized with respect to the disordered core size, and it is subsequently applied to determining the parameters of the model. In §5, we analyse the free boundary problem with the director field $\mathbf{n}$ and the graph of the boundary of the disordered core as unknowns. We show that the Lagrangian of the energy function is polyconvex for which lower semicontinuity and existence of minimizer of the total energy can be established. We finally show uniqueness of minimizer, with the azimuthal, spool-like configuration being the one of the lowest energy. We estimate the shape of the inner disordered core in the case that the bending effects dominate and show that it is never spherical (except when the energy involves surface tension only). The paper closes with concluding remarks in §6.

Let us conclude the introduction stating the Oseen–Frank energy of nematic liquid crystals. Let $\mathbf{n} \in \mathcal{S}^2$, that is, a unit vector field. The total energy of a nematic liquid crystal occupying a domain $\mathcal{U} \subset \mathbf{R}^3$ is given by $E(\mathbf{n}) = \int_{\mathcal{U}} W_{\mathrm{OF}}(\mathbf{n}, \nabla\mathbf{n})\,\mathrm{d}\mathbf{x}$,

$$\begin{aligned} 2W_{\mathrm{OF}}(\mathbf{n}, \nabla\mathbf{n}) = \int_{\mathcal{U}} \big\{ & K_1(\nabla\cdot\mathbf{n})^2 + K_2(\mathbf{n}\cdot\nabla\times\mathbf{n})^2 + K_3|\mathbf{n}\times\nabla\times\mathbf{n}|^2 \\ & + (K_2+K_4)\big(\mathrm{tr}(\nabla\mathbf{n})^2 - (\nabla\cdot\mathbf{n})^2\big)\big\}\,\mathrm{d}\mathbf{x}, \end{aligned} \tag{1.1}$$

where the Frank elasticity constants satisfy the inequalities,

$$K_1 > 0, K_2 > 0,\ K_3 > 0, K_2 \geq |K_4|, 2K_1 \geq K_2 + K_4. \tag{1.2}$$

2. Lyotropic chromonic liquid crystals

The hexagonal columnar phase of chromonic liquid crystals can be characterized by an orthonormal set of vectors $\{\mathbf{n}, \mathbf{m}, \mathbf{p}\}$, the director $\mathbf{n}$ describing the average direction of alignment of the columnar axes, and the remaining pair of lattice vectors encoding the geometry of the orthogonal cross-section. The energy involves three main contributions, one associated with the director $\mathbf{n}$, postulated as the Oseen–Frank energy of the nematic phase, subject to constraints. A second contribution, relevant to domains with free boundary, is the surface energy that expresses the cohesive property of the material in the columnar phase. The third contribution penalizes the distortion of the cross-sectional lattice points is a two-dimensional, solid-like, elastic energy function. Let the material parameters satisfy $K_3, \sigma > 0$ and set the saddle splay constant $K_4 = 0$ in

the Oseen–Frank energy. In a domain Ω, with free boundary $\partial\Omega$, we have

$$E_{\text{chr}} = \int_{\Omega} \left(K_3 |\mathbf{n} \times \nabla \times \mathbf{n}|^2 + \mathcal{W}_{\text{Hex}}(\nabla \mathbf{u}) \right) \mathrm{d}\mathbf{x} + \sigma \,\text{Area}(\partial\Omega), \tag{2.1}$$

$$|\mathbf{n}| = 1, \tag{2.2}$$

$$\nabla \cdot \mathbf{n} = 0 \text{ in } \Omega, \quad \mathbf{n} \cdot \nabla \times \mathbf{n} = 0 \text{ in } \Omega, \tag{2.3}$$

$$\mathbf{n} \cdot \boldsymbol{\nu} = 0 \text{ on } \partial\Omega, \tag{2.4}$$

$$\text{Vol}(\Omega) = V_0, \tag{2.5}$$

with V_0 constant and where $\mathbf{u} \in \text{span}\{\mathbf{m}, \mathbf{p}\}$ represents the plane displacement vector. The positive constants K_3 and σ denote the bending and surface tension moduli, respectively. The boundary condition (2.4) is still assumed if the boundary is fixed, in which case the constraint (2.5) becomes obsolete. The first and third terms, together with the constraints and ignoring $\mathcal{W}_{\text{Hex}}$, have been applied in the experimental studies of chromonic domains [2,7], formed by DSCG and Sunset Yellow, where the elastic energy does not seem to be relevant due to the very weak elastic moduli of those materials [6]. Well-known forms of $\mathcal{W}_{\text{Hex}}$ can be found in the works by de Gennes and Kléman [22,30], appropriate to small displacements and bending deformations, followed by the nonlinear elastic expressions by Oswald & Pieransky [31]. The role of $\mathcal{W}_{\text{Hex}}$ becomes more prominent in applications to DNA clustering. In this work, we propose an alternate form of $\mathcal{W}_{\text{Hex}}$ appropriate to materials made of (DNA) elastic filaments. Also, an alternate free energy expression to account for the cohesiveness of the columnar phase has been used in studies of DNA packing [32].

The role of the constraints is to express the large resistance to splay and twist deformation of the molecules. Specifically, splay of a liquid crystal is zero whenever dislocations do not occur, that is, the same number of filaments that enter a unit area exit that cross-section. In the case of the hexagonal columnar phase, non-zero splay would allow for deviations from the lattice structure. Twist is prohibited because of its incompatibility with the two-dimensional lattice order in planes perpendicular to the director. Setting $\nabla \cdot \nabla \times \mathbf{n} \equiv 0$ is a necessary and sufficient condition for the envelopes of the director to be perpendicular to a family of surfaces. An approximation to the constraint model can be achieved through relaxation. That is, to take into account the dominance of the splay and twist constants over the bending one by requiring

$$K_1,\ K_2 \gg K_3. \tag{2.6}$$

In §5, the relaxed form of the constraints (2.6) is used, instead of the exact requirement.

We propose a form of $\mathcal{W}_{\text{Hex}}$, partially motivated by the energy of smectic liquid crystals, that takes into account the elastic material being made of filaments. Let us then assume that

$$\mathcal{W}_{\text{Hex}}(\mathbf{n}, \mathbf{m}, \mathbf{p}) = \int_{\Omega} \left\{ B|\nabla(\mathbf{m} - \mathbf{p})|^2 + C|\nabla(\mathbf{m} + \mathbf{p})|^2 \right\} \mathrm{d}\mathbf{x} \tag{2.7}$$

and

$$\mathbf{m} = \mathbf{n} \times \mathbf{p}, \mathbf{n} \cdot \mathbf{p} = 0, |\mathbf{m}| = 1 = |\mathbf{p}| = |\mathbf{n}|, \tag{2.8}$$

where the constants $B > 0$ and $C > 0$ represent shear and compressible moduli, respectively. The expression (2.7) has been obtained from the hexagonal energy proposed by de Gennes ([22,23]) which is formulated in terms of the displacement vector $\mathbf{u}$ associated with deformations in the lattice plane. Such an energy contains two terms, penalizing the shearing and compression of the lattice. In our case, we have used the same energy but expressing $\mathbf{u}$ in terms of the lattice vectors, and have taken into account the constraints in (2.8). The latter has the effect of suppressing lower order terms in $\mathbf{m}$ and $\mathbf{p}$ (that is, non-gradient terms). We also arrived at our energy expression starting from the energy of the smectic A, in the case that two families of orthogonal layers (perpendicular to the lattice vectors) are present in the material, and with the DNA filament determined by their intersections.

royalsocietypublishing.org/journal/rsta Phil. Trans. R. Soc. A 379: 20200111

We conclude this section recalling a fundamental result in the analysis of energy minimization of nematic liquid crystals.

Theorem 2.1 ([33]). *Let $\mathcal{U} \in \mathbf{R}^3$ be an open and bounded set, with Lipschitz boundary $\partial\mathcal{U}$. Suppose that the Frank constants satisfy the inequalities (1.2). Let the admissible set be*

$$\mathcal{A}(\boldsymbol{n}_0) = \{\boldsymbol{n} \in H^1(\mathcal{U}, \mathcal{S}^2) : \text{ trace of } \boldsymbol{n} = \boldsymbol{n}_0\}$$

is non-empty. Then for any Lipschitz function $\boldsymbol{n}_0 : \partial\mathcal{U} \longrightarrow \mathcal{S}^2$, the functional $E(\boldsymbol{n}) = \int_{\mathcal{U}} W_{OF}(\boldsymbol{n}, \nabla\boldsymbol{n})\, d\boldsymbol{x}$ admits a minimizer in $\mathcal{A}(\boldsymbol{n}_0)$. Furthermore, if $\boldsymbol{n}$ is a minimizer of $E(\cdot)$, then $\boldsymbol{n}$ is analytic on $\mathcal{U}/Z$ for some relatively closed subset Z of $\mathcal{U}$ which has one-dimensional Hausdorff measure zero.

Remark 2.2. It is important to emphasize that the inequalities (1.2) guarantee the coercivity of $E(\mathbf{n})$.

Remark 2.3. Let us consider the energy $\mathcal{W}_{\text{Hex}}$ in the case that $\mathbf{p}$ is a prescribed constant vector, $\mathbf{p} = \mathbf{e}_z$. Steps analogous to those that lead to the conclusion of theorem 2.1 also prove the existence and partial regularity of minimizers of the energy $E = \int_{\mathcal{U}} \{W_{\text{OF}}(\mathbf{n}, \nabla\mathbf{n}) + \mathcal{W}_{\text{Hex}}(\mathbf{m}, \nabla\mathbf{m})\}\, d\mathbf{x}$, in the admissible set $\mathcal{A}_H = \{\mathbf{n}, \mathbf{m} \in H^1(\mathcal{U}, \mathcal{S}^2) : \text{ trace of } \mathbf{n} = \mathbf{n}_0, \text{ trace of } \mathbf{m} = \mathbf{m}_0, \text{ subject to (2.8)}\}$, for a given pair of unit vector fields, $\mathbf{m}_0$, $\mathbf{n}_0 \in H^1(\mathcal{U})$, satisfying $\mathbf{m}_0 \cdot \mathbf{n}_0 = 0$.

(a) DNA toroidal clusters

We consider a special class of energy minimizers of the problem (2.1)–(2.5) and construct some examples. First, we recall that a universal or general equilibrium configuration is an orientation pattern which may occur in the absence of externally applied body forces, regardless of the form of an admissible energy density $W(\mathbf{n}, \nabla\mathbf{n})$ [34]. For the Oseen–Frank energy W_{OF} and for all values of K_i, Marris [35] found that the set of universal solutions includes vector lines arranged in concentric circles. They are critical points of the Oseen–Frank energy (1.1) in the bulk, and, in particular of the problem (2.1)–(2.5).

Let as consider a toroidal domain, Ω, formed by revolving an elliptic disc, with semiaxes $a > 0$ and $b > 0$, and perpendicular to the xy-plane, about the z-axis. The radii $R, r > 0$ are as shown in (figure 3). Let us consider the new set of toroidal coordinates (r, γ, θ) defined as

$$x = (R + r\cos\gamma)\cos\theta, \quad y = (R + r\cos\gamma)\sin\theta, \; z = r\sin\gamma; \; 0 \le \theta, \gamma \le 2\pi. \tag{2.9}$$

We assume that the director field lines follow plane, concentric circles as $\mathbf{n} = (-\sin\theta, \cos\theta, 0)$. A long but straightforward calculation brings the total energy (2.1) to the form

$$E = K_3 \frac{2\pi^2 ab}{R + \sqrt{R^2 - b^2}} + \sigma\left(8\pi a R E_e\left(\sqrt{1 - \frac{b^2}{a^2}}\right)\right), \tag{2.10}$$

subject to the constraint $\text{Vol}(\Omega) = 2\pi^2 abR = V_0$. This constraint, along with the natural requirement that $a \ge b \ge d/2$, where d is the diameter of a DNA segment, dictates the following restrictions to be satisfied by the remaining parameters: $a = V_0/2\pi^2 bR$, $d/2 \le b \le R$, $b \le R \le 2V_0/\pi^2 d^2$. Here, $E_e(k)$, $k^2 := 1 - (b^2/a^2)$ is the complete elliptic integral of the second kind. Upon using the previous relations between a, b and R, we arrive at expressing the energy (2.10) as $E = E(b, R)$. We summarize the results of its minimization in the following table (the unit of length is nm): (see table 1) We find that the value $\sigma/K_3 = 0.05\,\text{nm}^{-1}$ gives the optimal values

$$a = 17.55\,\text{nm}, \; b = 16.77\,\text{nm} \quad \text{and} \quad R = 33.83\,\text{nm},$$

which correspond to a torus with outer and inner radii 101.2 nm and 34.1 nm, respectively. This agrees with the dimensions of the shapes reported in [7], indicating that the bending energy dominates over the surface one in DNA toroidal aggregates.

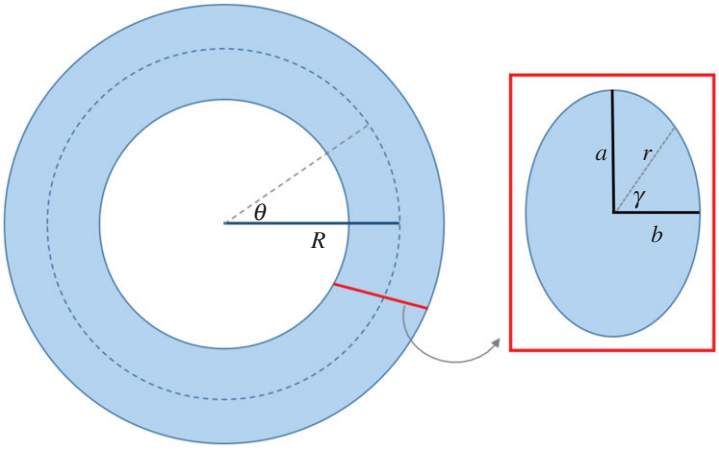

Figure 3. Toroidal domain Ω. (Online version in colour.)

Table 1. Dimensions of tori formed for different ratios of K_3/σ.

K_3/σ	a	b	R
$K_3 = 0, \sigma = 1$	29.2520	18.4460	18.4460
0.1	28.9096	18.5516	18.5582
1.0	26.6371	19.1047	19.5584
5.0	22.2264	19.0459	23.5120
10.0	19.8736	18.1872	27.5370
$K_3 = 1, \sigma = 0$	1.4000	1.4000	5077.7112

Likewise, taking $\sigma/K_3 = 20\,\mathrm{nm}^{-1}$, we arrive at the optimal values

$$a = 29.22\,\mu\mathrm{m}, \quad b = 18.45721\,\mu\mathrm{m} \quad \text{and} \quad R = 18.45727\,\mu\mathrm{m},$$

with the centre hole having practically disappeared as observed in experimental reports on Sunset Yellow chromonic liquid crystals [2]. We corroborate the trend indicating that in toroidal shapes of the latter, the surface energy dominates over bending in (3.1). However, we caution that the scope of domain formation in LCLCs is very complicated, with the previous finding showing only a very partial outlook.

3. DNA encapsidation

We now develop and analyse a model of DNA encapsidation based on the energy form (2.1) together with the constraints (2.2)–(2.4), with the appropriately modified volume relation, given below in (3.2). We include a bulk energy penalty of the disordered core, that is now an unknown of the proposed free boundary problem. We develop a strategy of parameter identification that includes information from Cryo-EM imaging.

We now describe our approach to modelling the packing of DNA within bacteriophage capsids using modelling techniques developed for liquid crystals. As mentioned in the previous section, the proposed model assumes that packed DNA forms chromonic liquid crystal phases. This is a natural assumption especially considering that chromonic liquid crystals are precisely named after DNA structures. Suppose $\mathcal{B}$ is the axisymmetric capsid domain and Ω_0 is the isotropic core region, an unknown of the problem. The domain containing the ordered liquid crystal phase

Table 2. Physical measurements of four different bacteriophages. The symbol L_p denotes the persistence length of a DNA chain of length L, effective diameter d, molar concentration c in a sphere-like capsid of radius R_c with a measured radius r_c of the disordered core. m_0 represents the linear density. T4 [36,37]; T5 [8]; T7 [38]; ϵ15 [39].

virus	L_p (nm)	d (nm)	c	L (nm)	R_c (nm)	r_c/R_c	m_0 (m^{-2})
T4	55.60	2.40	21.37	55047.6	40.00	0.5500	0.550×10^{17}
T5	58.38	2.94	17.85	39423.8	42.00	0.4286	1.693×10^{17}
T7	52.88	2.60	18.17	12932.0	26.05	0.5889	2.212×10^{17}
ϵ15	53.90	2.55	13.98	12846.0	28.37	0.5735	0.574×10^{17}

is defined as $\Omega := \mathcal{B} \setminus \Omega_0$. Then, to take into account the cross-sectional elastic energy (2.7), we modify the form (2.1) to

$$E_{\text{cap}} = \int_\Omega K_3 |\mathbf{n} \times \nabla \times \mathbf{n}|^2 \, \mathrm{d}\mathbf{x} + B|\nabla(\mathbf{m}+\mathbf{p})|^2 \\ C|\nabla(\mathbf{m}-\mathbf{p})|^2 + \nu \mathrm{Vol}(\Omega_0) + \sigma \mathrm{Area}(\partial\Omega_0) \tag{3.1}$$

and

$$\mathrm{Vol}(\Omega) + \mathrm{Vol}(\Omega_0) = \mathrm{Vol}(\mathcal{B}). \tag{3.2}$$

(2.2)–(2.4). The positive constants ν represents the isotropic moduli of the DNA, that accounts for the energy of the disordered DNA in the inner core. Substituting the constraint (3.2) directly into the energy, dividing through by K_3 and dropping the constant term vol($\mathcal{B}$), we get

$$E_{\text{cap}} = K_3 \left\{ \int_\Omega \left(|\mathbf{n} \times \nabla \times \mathbf{n}|^2 + \frac{B}{K_3}|\nabla(\mathbf{m}+\mathbf{p})|^2 + \frac{C}{K_3}|\nabla(\mathbf{m}-\mathbf{p})|^2 - \frac{\nu}{K_3} \right) \mathrm{d}\mathbf{x} \right. \\ \left. + \frac{\sigma}{K_3}\mathrm{Area}(\partial\Omega_0) \right., \tag{3.3}$$

with constraints (2.2)–(2.4), together with the orthogonality relations $\mathbf{m} = \mathbf{n} \times \mathbf{p}$, $\mathbf{n} \cdot \mathbf{p} = 0$, $|\mathbf{m}| = 1 = |\mathbf{p}|$.

From now on, we restrict ourselves to studying azimuthal configurations around the axis of the capsid, $\mathbf{p} = \mathbf{e}_z$. Using the identity $(\mathbf{n} \cdot \nabla \times \mathbf{n})^2 + |\mathbf{n} \times \nabla \times \mathbf{n}|^2 + \mathrm{tr}(\nabla\mathbf{n})^2 = |\nabla\mathbf{n}|^2$, the energy function (3.3) becomes

$$E_{\text{cap}} = A \int_\Omega \left(|\mathbf{n} \times \nabla \times \mathbf{n}|^2 + K\left(\mathrm{tr}(\nabla\mathbf{n})^2 + (\mathbf{n} \cdot \nabla \times \mathbf{n})^2 \right) - \frac{\nu}{A} \right) \mathrm{d}\mathbf{x} + \frac{\sigma}{A}\mathrm{Area}(\partial\Omega_0), \tag{3.4}$$

where

$$A = K_3 + B + C, \quad K = 1 - \frac{K_3}{A}. \tag{3.5}$$

The energy of the problem involves four effective parameters A, K, ν and σ, with the first one giving the energy scale. Next, we describe our strategy to estimate parameter values relevant to bacteriophage viruses. Following Tzlil *et al.* [11] and subsequently [32], we take the bending constant K_3 as

$$K_3 = K_B T L_p m_0, \tag{3.6}$$

where L_p denotes the persistence length of the DNA and m_0 its length density, with dimensions of one over the square of the length. For instance, for the T4-virus, we estimate $m_0 = 1/(\pi(d/2)^2) = 3.183 \times 10^{17}\ \mathrm{m}^{-2}$, with values for other viruses also shown in table 2.

We take guidance from the theory of Onsager for lyotropic liquid crystals, in order to obtain estimates for the isotropic modulus ν and the surface tension σ, and assume that they are functions of the (DNA) molar concentration c (rather, its dimensionless form, scaled by the factor

$4/(\pi d L_p^2)$) [24]. We then adopt the expressions

$$\nu = \nu_0(c)\frac{K_BT}{R_c^3} \quad \text{and} \quad \sigma = \sigma_0(c)\frac{K_BT}{L_p d}. \tag{3.7}$$

We assign the diameter d of the DNA and its persistence length L_p to those of a rod-like molecule, respectively, of the original Onsager theory. In particular, the form of σ corresponds to the surface tension modulus of rigid rods between the nematic and isotropic phases. This seems appropriate to the present problem since we also encounter a surface separating an ordered region from a disordered one.

To the best of our knowledge, there is no theory that establishes the forms of the scaling coefficients $\nu_0(c)$ and $\beta(c)$, even for lyotropic liquid crystals. However, many works in the literature derive estimates valid in certain rod concentration regimes [40]. For instance, in the case of large concentration of rods, Onsager derived the form $\nu_0 = \ln(c/4\pi) - 1 + c$ [24]. Likewise, for rod systems in the same high concentration regime, σ can be approximated as $\sigma = K_BT(0.257/L_p d)$ [41].

In order to find the appropriate range of values for the parameters B and C, we refer to data on experimentally measured values of the pressure inside the capsid, near the wall. We first estimate such pressure values for different viruses (§4), in the case $B = 0 = C$, that is, ignoring the transversal elastic energy $\mathcal{W}_{\text{Hex}}$. This yields the quantities P_0 shown in table 2, differing in a factor between 100 and 1000 from experimentally measured values. We address such an issue, by including the role of $\mathcal{W}_{\text{Hex}}$. For this, we appeal to the expressions proposed by Kléman & Lavrentovich, for columnar liquid crystals ([23], ch. 5), where the orders of magnitude of the transverse elastic moduli are compared to K_3. In our case, this argument leads to the relations

$$B + C = \delta K_3, \quad \delta := \left(\mu + \alpha\left(\frac{R_c}{d}\right)^2\right). \tag{3.8}$$

(Recall that R_c denotes the capsid radius and d the DNA diameter). We find that, to arrive at the orders of magnitude of the experimentally predicted pressure values, we must take α between 0.1 and 10, varying among the viruses under consideration. For instance, in terms of δ and for the T4-virus, we find that $\delta = 2.8 \times 10^2$. The expressions $A = (1+\delta)K_3$ of the energy scale) and $K = \delta/(1+\delta)$ in (3.5) immediately follow from (3.8). In §4, we calculate the pressure near the surface of the capsid and show that is proportional to A, as expected. This provides the second source of information to complete the selection of parameters.

4. Optimal spheroidal core size and pressure parameter studies

The goal of this section is to apply the previously developed model to predict the size of the spheroidal core region of disordered DNA at the centre of the bacteriophage capsid. The purpose of choosing a simple geometric setting is to provide model validation and a parameter assessment. We will first neglect the cross-sectional elastic energy in the model. This will lead to good predictions of the core size but yield pressure values near the capsid surface of two orders of magnitude smaller than the experimentally measured ones. We will conclude the section calculating the pressure corrections upon including the cross-sectional free energy.

We take the capsid $\mathcal{B}$ to be a sphere of dimensionless radius 1, truncated at the poles, at a distance $0 < h < 1$, $h \approx 1$, from the equator. We assume that the core Ω_0 is a truncated prolate spheroid with semiaxes $0 < a < 1$ and 1, respectively, with a being the unknown of the problem. Its cross-section in the $xz-$plane is given by the truncated ellipse $(x^2/a^2) + z^2 = 1$. Their representations in cylindrical coordinates are

$$\mathcal{B} = \left\{(r,\theta,z):\ 0 \le r \le \sqrt{1-z^2},\ 0 \le \theta < 2\pi, -h \le z \le h\right\}$$

and

$$\Omega_0 = \{(r,\theta,z):\ 0 \le r \le r_c(z),\ 0 \le \theta < 2\pi, -h \le z \le h\},$$

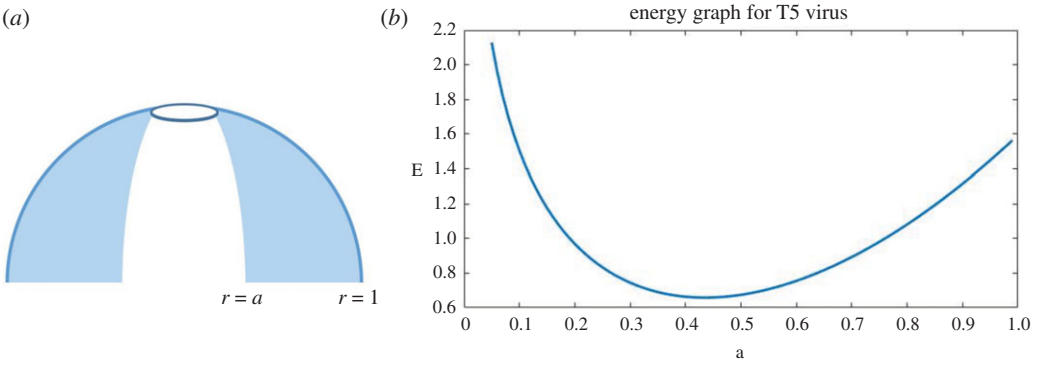

Figure 4. Prescribed capsid geometry (*a*). Energy plot for the T5 virus (*b*). (Online version in colour.)

Table 3. The quantities ν_0 and σ_0 represent dimensionless forms of the isotropic and surface moduli as in (3.7). The values shown are obtained by parameter fitting so that the disordered core size r_c predicted by the model (given in §4 as the dimensionless quantity a) falls into the range of values r_c experimentally obtained from Cryo-imaging analysis. The pressure P_0 shown in this table has been calculated with the model that ignores the columnar transverse energy (§4), resulting in values of order of magnitude 0.01 of those reported in experimental measurements [42].

virus	ν_0	σ_0	P_0 (*atm*)	r_c exp (nm)	r_c model (nm)	error (%)
T4	23.19	0.388	2.9	22.00	22.80	3.5
T5	19.04	0.228	5.5	17.64	21.48	17
T7	19.82	0.592	3.1	15.34	16.15	5.0
ϵ15	15.37	0.499	3.1	16.25	16.17	0.5

with $r_c = a\sqrt{1-z^2}$. The surface area of the truncated spheroid with semi-axes $\{a, b = 1\}$ is

$$\text{Area}\,(\partial\Omega_0) = 2\pi a^2\left(1 + \frac{1}{a\sqrt{1-a^2}}\arcsin\left(\sqrt{1-a^2}\right)\right) - 2\pi(1-h). \tag{4.1}$$

Let $\Omega = \mathcal{B} \setminus \Omega_0$ denote the dimensionless region where the DNA is ordered. The DNA configuration is assumed to be a azimuthal which is concentric in the xy-plane about the z-axis so that $\mathbf{n} = \mathbf{e}_\theta$ almost everywhere, where $\{\mathbf{e}_r, \mathbf{e}_\theta, \mathbf{e}_z\}$ is the standard basis for $\mathbb{R}^3$ in cylindrical coordinates. The total energy restricted to the given domains is (3.2), and taking into account that the domains Ω, $\mathcal{B}$ and Ω_0 are dimensionless, is

$$\begin{aligned} E_{\text{cap}}(a) &= \int_\Omega \left(K_3|\mathbf{n}\times\nabla\times\mathbf{n}|^2 - \nu\right)\mathrm{d}\mathbf{x} + \sigma\,\text{Area}(\partial\Omega_0) \\ &= K_3\left\{\int_{-h}^{h}\int_{a\sqrt{1-z^2}}^{\sqrt{1-z^2}}\int_0^{2\pi}\left(\frac{1}{2r} - \frac{\nu}{K_3}r\right)\mathrm{d}\theta\,\mathrm{d}r\,\mathrm{d}z + \frac{\sigma}{K_3}\text{Area}(\partial\Omega_0)\right\} \\ &= K_3\pi h\left\{\ln\left(\frac{1}{a}\right) - \frac{\nu}{K_3}h_1(a) + \frac{\sigma}{K_3}h_2(a)\right\} + \mathcal{O}(1-h) \end{aligned} \tag{4.2}$$

and

$$h_1(a) := \left(1 - \frac{1}{12}h^2\right)(1-a^2), \quad h_2(a) := \frac{2a}{h}\left(a + \frac{1}{\sqrt{1-a^2}}\arcsin\left(\sqrt{1-a^2}\right)\right). \tag{4.3}$$

The energy function (4.2) for data corresponding to the T5-virus is shown in figure 4. Calculations of the energy minimizing value a for several viruses are shown in table 2 (see table 3).

Let us now consider the energy (4.2) and estimate the pressure near the capsid wall for the azimuthal configuration $\mathbf{n} = \mathbf{e}_\theta$. For this, we calculate the variation of the energy (3.4) with respect

to **x** which yields the elastic forces. As expected, we find the value $P_0(r) := K_3/r^2$, when cross-sectional forces are neglected. In particular, the dimensional expression for the pressure at the capsid surface is $P_0(R_c) = K_b T m_0 (L_p/R_c^2)$. The values found for different viruses are shown in table 2. As previously mentioned, the pressure P_0, as calculated here, is under-predicted by about a factor of 100 (see table 3). The adjustment of K_3 as $A = (1+\delta)K_3$, leading to the same scaling for $P = (1+\delta)P_0$, provides the value $(1+\delta)$ required to bring the pressure to the experimentally measured range. This completes the evaluation of the model parameters.

5. Free inner boundary

In this section, we study the well-posedness of the free boundary problem corresponding to the energy (3.1) for axisymmetric domains. Images of bacteriophage viruses portray axisymmetric capsids and disordered core regions, often faceted. Here, we ignore the facet structures and consider smooth domains. A goal of the analysis is to justify the spooling assumption often made in viral studies, and, in particular, as in the previous section. We also ignore possible defects in the director field **n**.

We consider a set of spherical coordinates $\{(r,\phi,\theta) : 0 \le r,\ 0 \le \phi \le \pi,\ 0 \le \theta \le 2\pi\}$ and the corresponding orthonormal basis $\{\mathbf{e}_r, \mathbf{e}_\phi, \mathbf{e}_\theta\}$. We let $\mathcal{C}_A(a,b)$ denote the space of absolutely continuous functions on the interval (a,b). We assume the capsid, $\mathcal{B}$, to be the unit sphere with centre at the origin, and open sets $\Omega, \Omega_0 \subset \mathcal{B}$, $\Omega \cap \Omega_0 = \emptyset$. Here, Ω denotes the upper half region where the DNA is ordered, and Ω_0, also an open set, represents the upper hemisphere of the disordered core. We assume that the contact surface between them is the graph of a function, represented in spherical coordinates by an positive function $p \in \mathcal{C}_A(\phi^*, \frac{\pi}{2})$, $p = p(\phi)$, $0 < \phi^* < \phi < \frac{\pi}{2}$, so that

$$\Omega = \left\{(r,\phi,\theta) :\ 0 < p(\phi) < r < 1,\ \phi^* < \phi < \frac{\pi}{2},\ 0 < \theta < 2\pi\right\} \tag{5.1}$$

and

$$\Omega_0 = \left\{(r,\phi,\theta) :\ 0 < r < p(\phi), 0 < \phi < \frac{\pi}{2},\ 0 < \theta < 2\pi\right\}. \tag{5.2}$$

We interpret the conical region corresponding to $0 < \phi < \phi^*$, subtending an arch of dimensionless length $0 < \epsilon^* << 1$, as the neck of the capsid, so that $\epsilon^*/\phi^* = O(1)$ approximately represents the radial length of that structure. Here, we ignore the neck's role as possible spooling site and note that it serves to prevent the singularity that would otherwise occur at $\phi = 0$. (A different interpretation of ϕ^* is given in [11], where it is being associated with an empty region on top of the disordered core, where the pressure approaches 0. The value $\phi^* = 0.005$ radians is assigned to the T4-virus.) We consider the relaxed form of the energy (3.1), given by

$$E_{\text{cap}} = \int_0^{2\pi}\int_{\phi^*}^{\pi/2}\int_{p(\phi)}^{1} W_{OF}(\mathbf{n}, \nabla\mathbf{n})\, r^2 \sin\phi \,\mathrm{d}r\,\mathrm{d}\phi\,\mathrm{d}\theta + \nu \mathrm{Vol}(\Omega_0) + \sigma\,\mathrm{Area}(\partial\Omega_0), \tag{5.3}$$

with the constants of the Oseen–Frank energy satisfying the relations (2.6). We again apply the volume constraint (3.2) directly into the energy (5.3) and suppress the constant capsid volume term to get

$$E_{\text{cap}} = \int_0^{2\pi}\int_{\phi^*}^{\pi/2}\int_{p(\phi)}^{1} (W_{OF}(\mathbf{n}, \nabla\mathbf{n}) - \nu)\ r^2 \sin\phi \,\mathrm{d}r\,\mathrm{d}\phi\,\mathrm{d}\theta + \sigma\,\mathrm{Area}(\partial\Omega_0). \tag{5.4}$$

Remark 5.1. We point out that, as a consequence of the inequalities (1.2), the functional E_{cap} is also coercive in $H^1(\Omega)$. Indeed, $W_{\text{OF}}(\mathbf{n}, \nabla\mathbf{n}) - \nu \ge k|\nabla\mathbf{n}|^2 - \nu$ holds, which implies that

$$\int_\Omega (W_{\text{OF}}(\mathbf{n}, \nabla\mathbf{n}) - \nu)\,\mathrm{d}\mathbf{x} \ge k\|\nabla\mathbf{n}\|^2_{L^2(\Omega)} - \nu\,\mathrm{Vol}(\mathcal{B}),$$

where $k > 0$ is the coercivity constant corresponding to W_{OF}.

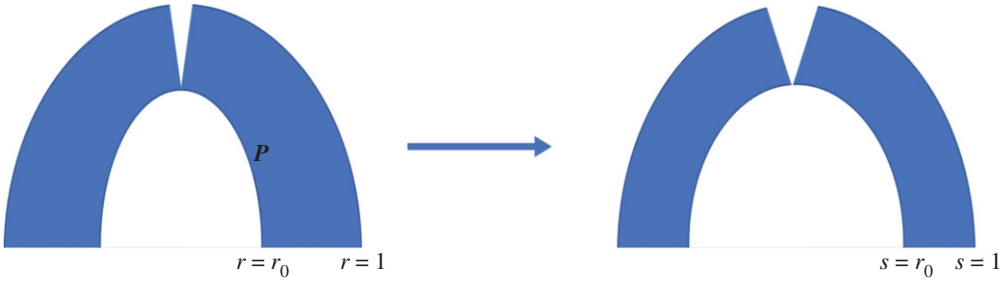

Figure 5. Visualization of coordinate change from free to fixed boundary. The parameter $r_0 > 0$ is an unknown. (Online version in colour.)

We consider liquid crystal configurations of the form $\mathbf{n} = \sin\varphi \mathbf{e}_\phi + \cos\varphi \mathbf{e}_\theta$, where $\varphi = \varphi(r, \phi)$ is the angle of the molecules at (r, ϕ, θ) from horizontal. The energy in terms of φ is the following

$$E_{\text{cap}} = \int_\Omega \{ \frac{K_1}{r^2} \left(\cos\varphi\varphi_\phi + \sin\varphi \frac{\cos\phi}{\sin\phi} \right)^2 + K_2 \varphi_r^2 \tag{5.5}$$

$$+ \frac{K_3}{r^2} + \frac{K_3}{r^2} \left(\sin\varphi\varphi_\phi - \cos\varphi \frac{\cos\phi}{\sin\phi} \right)^2 - \nu \Big\} \, r^2 \sin\phi \, \mathrm{d}r\mathrm{d}\phi\mathrm{d}\theta \tag{5.6}$$

$$+ 2\pi\sigma \int_{\phi^*}^{\pi/2} p\sqrt{p^2(\phi) + (p'(\phi))^2} \sin\phi \, \mathrm{d}\phi. \tag{5.7}$$

Next, we carry out a nonsingular change of variables that transforms the free boundary into a fixed one. A new radial coordinate s is defined so that the outer radius $r = 1$ remains fixed and the inner one is mapped to a constant radius r_0, as in figure 5. We let r_0 so that $1 > r_0 = \epsilon^*/\phi^* > 0$, where ϕ^* and ϵ^* are given in (5.2) and the paragraph thereafter. Specifically, let

$$\frac{\partial s}{\partial r} = c(1 - r) \implies s(r) = -c_1(1 - r)^2 + c_2 \tag{5.8}$$

and

$$s(p) = r_0 \ \& \ s(1) = 1 \implies c_1 = \frac{1 - r_0}{(1 - p)^2}, \ c_2 = 1. \tag{5.9}$$

Therefore, $s = 1 - (1 - r_0)(1 - r)^2/(1 - p)^2$ and the new coordinates (s, ϕ, θ) are related to the previous ones (r, ϕ, θ) by

$$r = 1 - \sqrt{(1 - s)(1 - p)^2/(1 - r_0)}, \quad \phi = \phi, \ \theta = \theta.$$

In these coordinates,

$$E_{\text{cap}} = \int_0^{2\pi} \int_{\phi^*}^{\pi/2} \int_{r_0}^1 (W_{OF}(\mathbf{n}, \nabla\mathbf{n}) - \nu) \ r^2(s) \frac{\partial r}{\partial s} \sin\phi \, \mathrm{d}s\mathrm{d}\phi\mathrm{d}\theta + \sigma \, \text{Area}(\partial\Omega_0). \tag{5.10}$$

With the coordinate transformation defined above and $\varphi(r, \phi) \mapsto \hat{\varphi}(s(r, \phi), \phi)$, then

$$\varphi_r = \hat{\varphi}_s \frac{\partial s}{\partial r}, \qquad \varphi_\phi = \hat{\varphi}_s \frac{\partial s}{\partial \phi} + \hat{\varphi}_\phi = \frac{2(1 - s)p'}{(1 - p)} \hat{\varphi}_s + \hat{\varphi}_\phi.$$

So the Oseen–Frank energy terms become

$$
\begin{aligned}
E_{\mathrm{cap}} = \int_\Omega \Bigg\{ & K_1 \left[\cos\hat{\varphi} \left(\hat{\varphi}_s \frac{\partial s}{\partial \phi} + \hat{\varphi}_\phi \right) + \sin\hat{\varphi} \cot\phi \right]^2 + K_2 r^2(s) \left(\hat{\varphi}_s \frac{\partial s}{\partial r} \right)^2 \\
& + K_3 + K_3 \left[\sin\hat{\varphi} \left(\hat{\varphi}_s \frac{\partial s}{\partial \phi} + \hat{\varphi}_\phi \right) - \cos\hat{\varphi} \cot\phi \right]^2 - \nu r^2(s) \Bigg\} \frac{\partial r}{\partial s} \sin\phi \, \mathrm{d}s\mathrm{d}\phi\mathrm{d}\theta \\
& + 2\pi\sigma \int_{\phi^*}^{\pi/2} p \sqrt{p^2(\phi) + (p'(\phi))^2} \, \sin\phi \, \mathrm{d}\phi \\
= \int_\Omega \Bigg\{ & K_1 \left[\cos\hat{\varphi} \left(\frac{-2(1-s)}{1-p} (-p'\hat{\varphi}_s) + \hat{\varphi}_\phi \right) + \sin\hat{\varphi} \cot\phi \right]^2 + \\
& + K_2 \left(\frac{2\sqrt{(1-r_0)(1-s)}}{1-p} - 2(1-s) \right)^2 \hat{\varphi}_s^2 \\
& + K_3 \left[\sin\hat{\varphi} \left(\frac{-2(1-s)}{1-p} (-p'\hat{\varphi}_s) + \hat{\varphi}_\phi \right) - \cos\hat{\varphi} \cot\phi \right]^2 \\
& - \nu \left(1 - \sqrt{\frac{1-s}{1-r_0}} (1-p) \right)^2 \Bigg\} \frac{\sin\phi(1-p)}{2\sqrt{(1-r_0)(1-s)}} \, \mathrm{d}s\mathrm{d}\phi\mathrm{d}\theta \\
& + \int_\Omega \frac{\sigma}{1-r_0} p \sqrt{p^2(\phi) + (p'(\phi))^2} \, \sin\phi \mathrm{d}s\mathrm{d}\phi\mathrm{d}\theta \qquad (5.11) \\
:= \int_\Omega & W_{\mathrm{cap}}(\hat{\varphi}_s, \hat{\varphi}_\phi, p', \varphi, p) \, \mathrm{d}s\mathrm{d}\phi\mathrm{d}\theta. \qquad (5.12)
\end{aligned}
$$

Let us now establish the boundary conditions to be satisfied by the fields of the problem.

$$
p\left(\frac{\pi}{2}\right) = r_0, \quad p'\left(\frac{\pi}{2}\right) = 0, \qquad (5.13)
$$

$$
\varphi(r, \phi^*) = \varphi\left(r, \frac{\pi}{2}\right) = 0, \quad r \in (p(\phi), 1) \qquad (5.14)
$$

and

$$
\varphi(1, \phi) = 0, \quad \frac{\partial \varphi}{\partial \boldsymbol{\nu}}(p, \phi) = 0, \quad \phi \in \left(\phi^*, \frac{\pi}{2}\right), \qquad (5.15)
$$

where $\boldsymbol{\nu}$ is the unit normal vector to the inner boundary $p = p(\phi)$. The first equation in (5.13) conveys the north pole structure of the capsid (i.e. the neck) into the bulk, and the second one expresses the symmetry of the whole configuration with respect to the equatorial plane. Equations (5.14) and (5.15) express the requirement that the director field be tangent to each, the outer and the inner boundary. These conditions reflect the fact that proteins in the capsid tend to enforce tangentiality of the DNA on the capsid boundary. We now set up the admissible set for the minimization of the energy. Let us fix $0 < \varepsilon$ arbitrarily small, and define the admissible sets for the relaxed and constraint problems, respectively,

$$
\mathcal{A}_\varepsilon = \left\{ (p, \varphi) \in H^1\left(\phi^*, \frac{\pi}{2}\right) \times H^1(\Omega) : \varepsilon < p < 1 - \varepsilon \text{ and } (5.13) - -(5.15) \text{ hold} \right\} \qquad (5.16)
$$

and

$$
\mathcal{A}_\varepsilon^c = \{ (p, \varphi) \in \mathcal{A}_\varepsilon : \nabla \cdot \mathbf{n} = 0 = \mathbf{n} \cdot \nabla \times \mathbf{n} \text{ in } \Omega \}. \qquad (5.17)
$$

We point out that both sets are non-empty. Indeed, the pair consisting of $\varphi = 0$ and $p(\phi) = r_0$ belongs to both sets. In order to prove the existence of a minimizing pair (p, φ), we need to assert the lower semicontinuity of the energy functional E_{cap} in $\mathcal{A}_\varepsilon$ and $\mathcal{A}_\varepsilon^c$. First of all, let us recall the following definition.

royalsocietypublishing.org/journal/rsta Phil. Trans. R. Soc. A 379: 20200111

Definition 5.2 ([43]). Consider the functional $I[u] = \int_{\mathcal{U}} L(x, \mathbf{z}, \mathbf{x})\, d\mathbf{x}$, $\mathcal{U} \subset \mathbb{R}^n$. A Lagrangian L is called polyconvex if L has the form

$$L(P, \mathbf{z}, \mathbf{x}) = F(P, \det P, \mathbf{z}, \mathbf{x}), \quad P \in M^{n\times n},\ \mathbf{z} \in \mathbb{R}^n,\ \mathbf{x} \in \mathcal{U}$$

and for each fixed $\mathbf{z}$, $\mathbf{x}$, the joint mapping $(P, r) \mapsto F(P, r, \mathbf{z}, \mathbf{x})$ is convex.

In order to apply the previous definition to our problem, we let

$$L = W_{\text{cap}}, \quad \mathbf{z} = (p, \hat{\varphi}), \quad \mathbf{x} = (s, \phi), \quad P = \begin{pmatrix} 0 & p'(\phi) \\ \hat{\varphi}_s & \hat{\varphi}_\phi \end{pmatrix}, \quad \det P = -p'\hat{\varphi}_s. \tag{5.18}$$

The following well-known lemma is needed in establishing necessary and sufficient conditions for the polyconvexity of the Lagrangian W_{cap}.

Lemma 5.3 ([43]). *Let f be a twice-differentiable function on an open convex set $U \subset \mathbb{R}^n$. Then $f(\mathbf{u}, \mathbf{x})$ is convex with respect to $\mathbf{u}$ on U if and only if its Hessian matrix is positive semidefinite for every $\mathbf{x} \in U$.*

Lemma 5.4. *The Lagrangian W_{cap} is polyconvex in $\mathcal{A}_\varepsilon$ and also in $\mathcal{A}_\varepsilon^c$.*

Proof. To show polyconvexity in $\mathcal{A}_\varepsilon$, we calculate the Hessian of $\tilde{W}_{\text{cap}}$ with respect to the variables $(p', \hat{\varphi}_s, \hat{\varphi}_\phi, -p'\hat{\varphi}_s)$, and show that the eigenvalues are nonnegative. Let

$$\ell := \frac{\sin\phi}{2\sqrt{(1-r_0)(1-s)(1-p)^2}}$$

Then, the non-zero terms of the Hessian are

$$\begin{aligned}
\frac{\partial^2 \tilde{W}_{cap}}{\partial p'^2} &= \frac{\sigma}{1-r_0}\frac{p^3}{(p^2+(p')^2)^{3/2}}\sin\phi,\\
\frac{\partial^2 \tilde{W}_{cap}}{\partial \hat{\varphi}_s^2} &= 8K_2\left(\sqrt{(1-r_0)(1-s)} - (1-s)(1-p)\right)^2 \ell,\\
\frac{\partial^2 \tilde{W}_{cap}}{\partial \hat{\varphi}_\phi^2} &= 2(1-p)^2(K_1\cos^2\hat{\varphi} + K_3\sin^2\hat{\varphi})\ell,\\
\frac{\partial^2 \tilde{W}_{cap}}{\partial \hat{\varphi}_\phi \partial(-p'\hat{\varphi}_s)} &= \frac{\partial^2 \tilde{W}_{cap}}{\partial(-p'\hat{\varphi}_s)\partial\hat{\varphi}_\phi} = -4(1-s)(1-p)(K_1\cos^2\hat{\varphi} + K_3\sin^2\hat{\varphi})\ell,\\
\frac{\partial^2 \tilde{W}_{cap}}{\partial(-p'\hat{\varphi}_s)^2} &= 8(1-s)^2(K_1\cos^2\hat{\varphi} + K_3\sin^2\hat{\varphi})\ell.
\end{aligned}$$

Therefore, replacing ℓ with its full expression, the matrix has eigenvalues

$$\begin{aligned}
\lambda_1 &= 0, \quad \lambda_2 = \frac{\sigma}{1-r_0}\frac{p^3}{(p^2+(p')^2)^{3/2}}\sin\phi,\\
\lambda_3 &= \frac{\sin\phi}{2\sqrt{(1-r_0)(1-s)(1-p)^2}} \cdot \left(8(1-s)^2 + 2(1-p)^2\right)(K_1\cos^2\hat{\varphi} + K_3\sin^2\hat{\varphi})
\end{aligned}$$

and

$$\lambda_4 = \frac{\sin\phi}{2\sqrt{(1-r_0)(1-s)(1-p)^2}} \cdot 8K_2\left(\sqrt{(1-r_0)(1-s)} - (1-s)(1-p)\right)^2,$$

where the $\sin\phi$ factor is strictly positive since $0 < \phi^* < \phi \le \frac{\pi}{2} - \phi^*$. Being that all of the eigenvalues are nonnegative, we can conclude that the Hessian is positive semidefinite. Hence, the result follows by lemma 5.3. The analogous conclusion for $\mathcal{A}_\varepsilon^c$ follows immediately from the previous calculation. ∎

Theorem 5.5. *Suppose that the inequalities (1.2) for the Frank constants hold. For each pair of constants ϵ^*, ϕ^* as in (5.2), there exist a minimizing pair $(\hat{\varphi}, \hat{p})$ of the energy (5.7) in the admissible set (5.16). Furthermore, $\hat{p} \in \mathcal{C}_A(\phi^*, \pi/2)$. The same conclusions hold for the analogous problem in $\mathcal{A}_\varepsilon^c$.*

Proof. Let $\{p_k, \varphi_k\}$ be a minimizing sequence in $\mathcal{A}_\varepsilon$ for the functional (5.11). By the coercivity of the functional and the fact that $\mathcal{A}_\varepsilon$ is non-empty, together with the Poincaré inequality, it follows that this sequence has bounded H^1 norm. So, it has a subsequence that converges weakly to a limit $(\hat{\varphi}, \hat{p}) \in H^1(\phi^*, \frac{\pi}{2}) \times H^1(\Omega)$ and, so, strongly in L^2. Since W_{cap} (5.11) is polyconvex, the corresponding energy is weakly lower semicontinuous. Hence $E_{\text{cap}}(\hat{p}, \hat{\varepsilon}) = \inf_{(p,\varphi)\in\mathcal{A}_\varepsilon} E_{\text{cap}}(p, \varphi)$. The absolute continuity of $\hat{p}(\phi)$ is an immediate consequence of the fact that $\hat{p} \in H^1(\phi^*, \frac{\pi}{2})$. Reversing the change of variables (5.9) the result applies to the energy in the form (5.7). The conclusions can be immediately applied to the problem in $\mathcal{A}_\varepsilon^c$. Indeed, by the properties of the minimizing sequences, formulated in vector form, for convenience, we have that $\nabla \cdot \mathbf{n}_j \rightharpoonup \nabla \cdot \hat{\mathbf{n}}$ and $\mathbf{n}_j \cdot \nabla \times \mathbf{n}_j \rightharpoonup \hat{\mathbf{n}} \cdot \nabla \times \hat{\mathbf{n}}$, as $j \to \infty$, hold. ∎

Let us now turn to the energy minimization problem under the constraints (2.3).

Corollary 5.6. *Suppose that the assumptions of theorem (5.5) hold. Let $(\hat{p}_j, \hat{\varphi}_j) \in \mathcal{A}_\varepsilon$) be a sequence of minimizers for E_{cap} in (5.7) with Frank constants $\{(K_1^j, K_2^j, K_3^j)\}$ satisfying (1.2) and such that $\lim_{j\to\infty} K_1^j = \infty$. Then there is a subsequence $(\hat{p}_{j^l}, \hat{\varphi}_{j^l}) \in \mathcal{A}_\varepsilon$ such that $\hat{p}_{j^l} \rightharpoonup p^\infty$ and $\hat{\varphi}_{j^l} \rightharpoonup \varphi^\infty$ as $j^l \to \infty$ where $(p^\infty, \varphi^\infty)$ satisfy $\nabla \cdot \boldsymbol{n}^\infty = \cos\varphi^\infty \varphi_\phi^\infty + \sin\varphi^\infty \cot\phi = 0$. The analogous result holds as $\lim_{j\to\infty} K_2^j = \infty$, where now the limit is twist free, that is, satisfies $\bar{\boldsymbol{n}}^\infty \cdot \nabla \times \bar{\boldsymbol{n}}^\infty = \bar{\varphi}_r = 0$.*

Proof. From the energy form (5.7), we obtain the following relation

$$\begin{aligned} &E_{\text{cap}}(\hat{p}_j, \hat{\varphi}_j) + \nu \text{Vol}(\Omega(\hat{p}_j, \hat{\varphi}_j)) \le E_{\text{cap}}(p, \varphi) + \nu \text{Vol}(\Omega(p, \varphi)) \\ &= \int_\Omega \left\{ \frac{K_1}{r^2} \left(\cos\varphi\varphi_\phi + \sin\varphi \frac{\cos\phi}{\sin\phi} \right)^2 \right. \\ &\quad + K_2 \varphi_r^2 + \frac{K_3}{r^2} + \frac{K_3}{r^2} \left(\sin\varphi\varphi_\phi - \cos\varphi \frac{\cos\phi}{\sin\phi} \right)^2 \Big\} r^2 \sin\phi \, \mathrm{d}r\mathrm{d}\phi\mathrm{d}\theta \\ &\quad + 2\pi\sigma \int_{\phi^*}^{\pi/2} p\sqrt{p^2(\phi) + (p'(\phi))^2} \sin\phi \, \mathrm{d}\phi. \end{aligned} \tag{5.19}$$

Taking the special pair from $\mathcal{A}_\varepsilon$ such that $\varphi = 0$ and substituting it on the right-hand side of the previous inequality, we get

$$\begin{aligned} &\int_\Omega \left\{ \frac{K_1{}^j}{r^2} \left(\cos\hat{\varphi}_j \hat{\varphi}_{j_\phi} + \sin\hat{\varphi}_j \frac{\cos\phi}{\sin\phi} \right)^2 + K_2^j \varphi_r^2 \right\} r^2 \sin\phi \, \mathrm{d}r\mathrm{d}\phi\mathrm{d}\theta \\ &\le \int_\Omega \frac{K_3^j}{r^2} \csc^2\phi \, r^2 \sin\phi \, \mathrm{d}r\mathrm{d}\phi\mathrm{d}\theta + 2\pi\sigma \int_{\phi^*}^{\pi/2} p\sqrt{p^2(\phi) + (p'(\phi))^2} \sin\phi \, \mathrm{d}\phi. \end{aligned} \tag{5.20}$$

The conclusions follow by separately taking limits as $K_1^j \to \infty$ and $K_2^j \to \infty$, respectively. ∎

Of course, the energy may have many critical points. A configuration of interest in this work is the planar, azimuthal, spool-like configuration $\mathbf{n} = \mathbf{e}_\theta$, which corresponds to $\varphi \equiv 0$. This solution satisfies the boundary conditions, splay and twist constraints, and the Euler–Lagrange equations for φ (omitted), and thus, the question of whether this configuration has the least energy begs to be addressed. In theorem 5.7, we show that it does indeed have the least energy among configurations that we consider.

This result was anticipated due to the fact that the packing is at near-crystalline density, which leaves little room for randomness in the configuration. Theoretical works done by experimentalists, such as [11,16,44], assume this configuration without remark. In fact, in theorem 5.7, we will demonstrate that even with weaker boundary information, as long as it is satisfied by $\mathbf{n} = \mathbf{e}_\theta$, the solution $\varphi \equiv 0$ will have lower energy than a non-constant minimizer φ^*, such that $\varphi_\theta^* \equiv 0$, when each is paired with a fixed free boundary p^* that corresponds with φ^*.

Theorem 5.7. *The function $\hat{\varphi} \equiv 0$ is the unique minimizer in $\mathcal{A}_\varepsilon^c$ for a given boundary function p^*. Moreover, for $0 \le \sigma << K_3, \nu$, the minimizing profile corresponding to $\hat{\varphi} \equiv 0$ is of the form*

$$\hat{p}(\phi) = \sqrt{\frac{K_3}{\nu}} \csc\phi + O\left(\frac{\sigma}{K_3}\right). \tag{5.21}$$

In particular, the spherical profile $p(\phi) = r_0$, constant, is the minimizer only in the case $K_3 = 0 = \nu$.

Proof. Suppose $(p^*, \varphi^*) \in \mathcal{A}_\varepsilon^c$ is a minimizing pair for $\tilde{E}_{cap}$ such that $\varphi^* \neq 0$. Suppose also that $\varphi_\theta^* \equiv 0$. Let $\mathbf{n}^* = \sin\varphi^* \mathbf{e}_\phi + \cos\varphi^* \mathbf{e}_\theta$. We first compare the energy for $\mathbf{n}^*$ with that of $\mathbf{e}_\theta = \sin(0)\mathbf{e}_\phi + \cos(0)\mathbf{e}_\theta$, ignoring the free boundary contribution:

$$\begin{aligned} E_{\text{cap}}(\mathbf{n}^*) - E_{\text{cap}}(\mathbf{e}_\theta) &= \int_\Omega K_3 \left\{ \left[1 + \left(\sin\varphi^* \varphi_\phi^* - \cos\varphi^* \cot\phi \right)^2 \right] - \left[1 + \cot^2\phi \right] \right\} \sin\phi \, \mathrm{d}r\mathrm{d}\phi\mathrm{d}\theta \\ &= K_3 \int_\Omega \left[\varphi_\phi^{*2} - \left(\cos\varphi^* \varphi_\phi^* + \sin\varphi^* \cot\phi \right)^2 \right] \sin\phi \, \mathrm{d}r\mathrm{d}\phi\mathrm{d}\theta \\ &= K_3 \int_\Omega |\nabla\varphi^*|^2 \, r^2 \sin\phi \, \mathrm{d}r\mathrm{d}\phi\mathrm{d}\theta \ \ge 0, \end{aligned}$$

and only equals zero if $\varphi^* \equiv 0$. Thus, $\varphi \equiv 0$ is the unique minimizer in $\mathcal{A}$ for a given p^*.

Therefore, what remains is to determine minimizing free boundary functions p that pair with $\varphi \equiv 0$, i.e. $\mathbf{n} = \mathbf{e}_\theta$. The energy is

$$\begin{aligned} E_{\text{cap}}(\mathbf{e}_\theta) &= K_3 \int_{\phi^*}^{\pi/2} \int_0^{2\pi} \int_{p(\phi)}^1 (\csc\phi - \nu r^2 \sin\phi) \, \mathrm{d}r\mathrm{d}\theta\mathrm{d}\phi + 2\pi\sigma \int_{\phi^*}^{\pi/2} p\sqrt{p^2 + (p')^2} \sin\phi \, \mathrm{d}\phi \\ &= \int_{\phi^*}^{\pi/2} \left(2\pi K_3 \csc^2\phi (1 - p) - \frac{2\pi\nu}{3}(1 - p^3) + 2\pi\sigma p\sqrt{p^2 + (p')^2} \right) \sin\phi \, \mathrm{d}\phi. \end{aligned} \tag{5.22}$$

To learn about minimizers, we find the Euler–Lagrange equation for p. To do so, we take fixed $q \in H_0^1(\phi^*, \pi/2)$ and let

$$\begin{aligned} i(\epsilon) = 2\pi \int_{\phi^*}^{\pi/2} \Bigg(& K_3 \csc^2\phi (1 - p - \epsilon q) - \frac{\nu}{3}\left(1 - (p + \epsilon q)^3\right) \\ & + \sigma (p + \epsilon q)\sqrt{(p + \epsilon q)^2 + (p' + \epsilon q')^2} \Bigg) \sin\phi \, \mathrm{d}\phi. \end{aligned}$$

Then,

$$i'(0) = 2\pi \int_{\phi^*}^{\pi/2} \left[-K_3 \csc^2\phi + \nu p^2 - \sigma \left(\frac{pp'}{\sqrt{p^2 + (p')^2}} \right)' + \sigma \frac{2p^2 + (p')^2 - pp'\cot\phi}{\sqrt{p^2 + (p')^2}} \right] q \sin\phi \, \mathrm{d}\phi$$

Therefore, any minimizing p must satisfy

$$K_3 \csc^2\phi = \nu p^2 - \sigma \left(\frac{pp'}{\sqrt{p^2 + (p')^2}} \right)' + \sigma \frac{2p^2 + (p')^2 - pp'\cot\phi}{\sqrt{p^2 + (p')^2}}. \tag{5.23}$$

The expression (5.21) follows immediately from the previous equation, by a boundary layer asymptotic analysis calculation, guaranteeing the first boundary condition in (5.13) to hold. (The second boundary condition is already satisfied by the leading term.) ∎

6. Conclusion

One main issue not treated in this article is the reconstitution of the DNA filament. Indeed, we note that the recovery of the filament from a minimizing set $\{\mathbf{n}, \mathbf{m}, \mathbf{p}\}$ is the Lagrangian version of the Eulerian problem studied here. In still unpublished work, the authors follow two different reconstruction approaches, one, from the point of view of non-smooth dynamical systems and transport problems, and the second one, using Monte Carlo methods.

In the future, we also envision applying methods of data science that would allow for a consistent and comprehensive parameter identification, specially in view of wider applications of phage technologies.

Data accessibility. This article has no additional data.

Authors' contributions. This paper follows, in part, the PhD thesis dissertation by the first author, Lindsey Hiltner (November 2018). The thesis was supervised by M.C.C. The biological aspects of the work have been advised by the two mathematics biology coauthors, J.A. and M.V.

Competing interests. We declare we have no competing interests.

Funding. M.C.C. and L.H. knowledge the support from the National Science Foundation, grant nos DMS-DMREF 1729589 and DMS-1816740. M.C.C. also knowledge the hospitality of the Isaac Newton Institute at Cambridge University, UK and the support from the Simmons Foundation. J.A. and M.V. acknowledge the support of the National Science Foundation, grant no. DMS-1817156.

References

1. Lydon J. 1998 Chromonic liquid crystal phases. *Curr. Opin. Colloid Interface Sci.* **3**, 458–466. (doi:10.1016/S1359-0294(98)80019-8)
2. Tortora L *et al.* 2010 Selfassembly, condensation and order in aqueous lyotropic chromonic liquid crystals crowded with additives. *Soft Matter* **6**, 4157–4167. (doi:10.1039/c0sm00065e)
3. Livolant F. 1978 Positive and negative birefringence in chromosomes. *Chromosoma* **68**, 45–58. (doi:10.1007/BF00330371)
4. Livolant F, Mangenot S, Leforestier A, Bertin M, Frutos Aand De, Raspaud E, Durand D. 2006 Are liquid crystalline properties of nucleosomes involved in chromosome structure and dynamics? *Phil. Trans. R. Soc. A* **364**, 2615–2633.
5. Marenduzzo D, Orlandini E, Stasiak A, Tubiana L, Micheletti C. 2009 Dna–dna interactions in bacteriophage capsids are responsible for the observed dna knotting. *Proc. Natl Acad. Sci. USA* **106**, 22 269–22 274. (doi:10.1073/pnas.0907524106)
6. Zhou S. 2017 Elasticity of lyotropic chromonic liquid crystals probed by director reorientation in magnetic field. In *Lyotropic Chromonic Liquid Crystals*, pp. 13–31. New York, NY: Springer.
7. Hud ID, Vilfan NVand. 2005 Toroidal dna condensates: unraveling the fine structure and the role of nucleation in determining size. *Annu. Rev. Biophys. Biomol. Struct.* **34**, 295–318. (doi:10.1146/annurev.biophys.34.040204.144500)
8. Effantin G, Boulanger P, Neumann E, Letellier L, Conway JF. 2006 Bacteriophage t5 structure reveals similarities with hk97 and t4 suggesting evolutionary relationships. *J. Mol. Biol.* **361**, 993–1002. (doi:10.1016/j.jmb.2006.06.081)
9. Poliakov A, van Duijn E, Lander G, Fu CY, Johnson JE, Prevelige PE, Heck AJ. 2007 Macromolecular mass spectrometry and electron microscopy as complementary tools for investigation of the heterogeneity of bacteriophage portal assemblies. *J. Struct. Biol.* **157**, 371–383. (doi:10.1016/j.jsb.2006.09.003)
10. Prevelige PE. 2010 Mind the gap:how some viruses infect their hosts. *Viruses* **2**, 2536–2540. (doi:10.3390/v2112536)
11. Tzlil S, Kindt JT, Gelbart WM, Ben-Shaul A. 2003 Forces and pressures in dna packaging and release from viral capsids. *Biophys. J.* **84**, 1616–1627. (doi:10.1016/S0006-3495(03)74971-6)
12. Liu T, Sae-Ueng U, Li D, Lander GC, Zuo X, Jönsson B, Rau D, Shefer I, Evilevitch A. 2014 Solid-to-fluid–like dna transition in viruses facilitates infection. *Proc. Natl Acad. Sci. USA* **111**, 14 675–14 680. (doi:10.1073/pnas.1321637111)
13. Citorik RJ, Mimee M, Lu TK. 2014 Bacteriophage-based synthetic biology for the study of infectious diseases. *Curr. Opin Microbiol.* **19**, 59–69. (doi:10.1016/j.mib.2014.05.022)
14. Rasmussen TS, Koefoed AK, Jakobsen R, Deng L, Castro-Mejía JL, Brunse A, Neve H, Vogensen FK, Nielsen DS. 2020 Bacteriophage-mediated manipulation of the gut microbiome-promises and presents limitations. *FEMS Microbiol. Rev.* **44**, 507–521.
15. Arsuaga J, Tan R, Vazquez M, Harvey S. 2002 Investigation of viral dna packaging using molecular mechanics models. *Biophys. Chem.* **101**, 475–484. (doi:10.1016/S0301-4622(02)00197-7)
16. Kindt J, Tzlil S, Ben-Shaul A, Gelbart WM. 2001 Dna packaging and ejection forces in bacteriophage. *Proc. Natl Acad. Sci. USA* **98**, 13 671–13 674. (doi:10.1073/pnas.241486298)

17. Petrov AS, Boz MB, Harvey SC. 2007 The conformation of double-stranded DNA inside bacteriophages depends on capsid size and shape. *J. Struct. Biol.* **160**, 241–248. (doi:10.1016/j.jsb.2007.08.012)
18. Svenšek D, Veble G, Podgornik R. 2010 Confined nematic polymers: order and packing in a nematic drop. *Phys. Rev. E* **82**, 011708. (doi:10.1103/PhysRevE.82.011708)
19. Svenšek D, Podgornik R. 2013 Confined chiral polymer nematics: ordering and spontaneous condensation. *EPL (Europhysics Letters)* **100**, 66005. (doi:10.1209/0295-5075/100/66005)
20. Shin GM, Grason H. 2011 Filling the void in confined polymer nematics:phase transitions in a minimal model of dsDNA packing. *EPL* **96**, 36007. (doi:10.1209/0295-5075/96/36007)
21. Walker S, Arsuaga J, Vázquez M, Calderer MC, Hiltner L. 2020 Liquid crystal model of viral dna encapsidation. *Phys. Rev. E* **101**, 022703. (doi:10.1103/PhysRevE.101.022703)
22. De Gennes PG, Prost J, Pelcovits R. 1995 The physics of liquid crystals. *Phys. Today* **48**, 67. (doi:10.1063/1.2808028)
23. Kleman M, Lavrentovich OD. 2003 *Soft matter physics*. New York, NY: Springer.
24. Onsager L. 1949 The effects of shape on the interaction of colloidal particles. *Ann. N Y Acad. Sci.* **51**, 627–659. (doi:10.1111/j.1749-6632.1949.tb27296.x)
25. Barberi L, Livolant F, Leforestier A, Lenz M. 2020 Local structure of dna toroids reveals curvature-dependent intermolecular forces. *bioRxiv*, 1–12. (https://hal.archives-ouvertes.fr/hal-03084486)
26. Liu P, Arsuaga J, Calderer MC, Golovaty D, Vazquez M, Walker S. 2020 Ion-dependent dna configuration in bacteriophage capsids.
27. Leforestier A, Livolant F. 2009 Structure of toroidal dna collapsed inside the phage capsid. *Proc. Natl Acad. Sci. USA* **106**, 9157–9162. (doi:10.1073/pnas.0901240106)
28. Cruz B, Zhu Z, Calderer MC, Arsuaga J, Vazquez M. 2020 Quantitative study of the chiral organization of the phage genome induced by the packaging motor. *Biophys. J.* **118**, 2103–2116.
29. Zhou S *et al.* 2012 Elasticity of lyotropic chromonic liquid crystals probed by director reorientation in a magnetic field. *Phys. Rev. Lett.* **109**, 037801. (doi:10.1103/PhysRevLett.109.037801)
30. Kleman M. 1980 Developable domains in hexagonal liquid crystals. *J. Phys.* **41**, 737–745. (doi:10.1051/jphys:01980004107073700)
31. Oswald P, Pieranski P. 2005 *Smectic and columnar liquid crystals: concepts and physical properties illustrated by experiments*. Boca Raton, FL: CRC Press.
32. Klug WS, Ortiz M. 2003 A director-field model of dna packaging in viral capsids. *J. Mech. Phys. Solids* **51**, 1815–1847. (doi:10.1016/S0022-5096(03)00071-1)
33. Hardt R, Kinderlehrer D, Lin FH. 1986 Existence and partial regularity of static liquid crystal configurations. *Commun. Math. Phys.* **105**, 547–570. (doi:10.1007/BF01238933)
34. Ericksen JL. 1967 General solutions in the hydrostatic theory of liquid crystals. *Trans. Soc. Rheol.* **11**, 5–14. (doi:10.1122/1.549087)
35. Marris AW. 1978 Universal solutions in the hydrostatics of nematic liquid crystals. *Arch. Rat. Mech. Anal.* **67**, 251–303. (doi:10.1007/BF00253150)
36. Mesyanzhinov VV. 2004 Bacteriophage t4: structure, assembly, and initiation infection studied in three dimensions. *Adv. Virus Res.* **63**, 287–352. (doi:10.1016/S0065-3527(04)63005-3)
37. Olson NH, Gingery M, Eiserling TS, Baker FA. 2001 The structure of isometric capsids of bacteriophage t4. *Virology* **279**, 385–391. (doi:10.1006/viro.2000.0735)
38. Cerritelli ME, Cheng N, Rosenberg AH, McPherson CE, Booy FP, Steven A. 1997 Encapsidated conformation of bacteriophage t7 dna. *Cell* **91**, 271–280. (doi:10.1016/S0092-8674(00)80409-2)
39. Jiang W, Chang J, Jakana J, Weigele P, King J, Chiu W. 2006 Structure of epsilon15 bacteriophage reveals genome organization and dna packaging/injection apparatus. *Nature* **439**, 612–616. (doi:10.1038/nature04487)
40. van Roij R. 2005 The isotropic and nematic liquid crystal phase of colloidal rods. *Eur. J. Phys.* **26**, S57. (doi:10.1088/0143-0807/26/5/S07)
41. Doi M, Kuzuu N. 1985 Structure of the interface between the nematic phase and the isotropic phase in the rodlike molecules. In *J. Appl. Polym. Sci.*, vol. 41, pp. 65–68.
42. Grayson P, Evilevitch A, Inamdar M, Purohit PK, Gelbart WM, Knobler CM, Phillips R. 2006 The effect of genome length on ejection forces in bacteriophage lambda. *Virology* **348**, 430–436. (doi:10.1016/j.virol.2006.01.003)
43. Evans LC. 1998 Partial differential equations. *Am. Math. Soc.* **2**, 1998.
44. Gelbart WM, Knobler CM. 2008 The physics of phages. *Phys. Today* **61**, 42–47. (doi:10.1063/1.2835152)